Journal of Applied Polymer Science

Novel floating photocatalysts based on polyurethane composite foams modified with silver/titanium dioxide/graphene ternary nanoparticles for the visible-light-mediated remediation of diesel-polluted surface water

Lingfeng Ni, Yi Li, Chi Zhang, Linze Li, Wenlong Zhang, Dawei Wang
Key Laboratory of Integrated Regulation and Resource Development of Shallow Lakes (Ministry of Education), College of Environment, Hohai University, Xikang Road 1, Nanjing 210098, People's Republic of China
Correspondence to: Y. Li (E-mail: envly@hhu.edu.cn)

ABSTRACT: Photocatalyst loading on a floating substitute is accepted as a promising method for the remediation of diesel-polluted surface water. Therefore, novel photocatalysts based on polyurethane foams modified with silver/titanium dioxide/graphene ternary nanoparticles (PU–Ag/P25/G) were synthesized and investigated. Scanning electron microscopy, energy-dispersive X-ray spectrometry, X-ray diffraction, Fourier transform infrared spectroscopy, and UV–visible spectroscopy showed the coexistence of Ag, Degussa P25 (P25), and graphene and the nanoscale dispersion of nanoparticles in the matrix and on the surface of the polyurethane (PU) foam. The diesel adsorption capacity of the photocatalyst reached 96 g/g. The maximum diesel degradation was found to be 76% in a period of 16 h. Compared with polyurethane-foam-supported P25/graphene (PU–P25/G) and polyurethane-foam-supported P25 (PU–P25), all of the adsorption isotherm and degradation kinetics followed the order PU–Ag/P25/G > PU–P25/G > PU–P25 > PU; this was due to the loading of different nanoparticles. Moreover, the degradation efficiency was reduced only 5% after five consecutive reactions; this showed good stability and reusability of the photocatalyst for surface water restoration. © 2016 Wiley Periodicals, Inc. J. Appl. Polym. Sci. **2016**, *133*, 43400.

KEYWORDS: adsorption; applications; degradation; foams; optical properties

Received 29 August 2015; accepted 2 January 2016
DOI: 10.1002/app.43400

INTRODUCTION

In recent years, the problems of oil spills worldwide have caused constant concern because of their ecological damage and environmental pollution. In addition to the release of toxic substances, oil spills, such as those of diesel, which is widely used as an important fuel, may cover the water surface, reduce photosynthesis of aquatic plants, and dissolve oxygen therein.[1–3] The extensive utilization of diesel and the emission of oily wastewater have caused increasingly serious pollution in harbor areas and river water bodies.[4,5]

Current remediation techniques for oil spills are typically classified as mechanical/physical, thermal, biological, and chemical.[6] With the rapid development of photocatalytic technology, photocatalysis has been accepted as a promising method for cleaning up spilled oil.[7–9] Photocatalysis has merits; it has a high efficiency, nontoxicity, and a lower secondary pollution, and it requires no additives and is relatively economical. In addition, photochemical transformations are extremely effective compared to other degradation mechanisms for recalcitrant compounds in oil spills.[10]

As a traditional photocatalyst, titanium dioxide (TiO_2) has been well studied for the degradation of organic pollutants, including spilled oil.[11–14] Among industrialized products, Degussa P25 (P25), a mixture of anatase (ca. 70%) and rutile (ca. 30%), is the one with the highest applicability because of its electronic properties, relative low costs, nontoxicity, and excellent physicochemical stability. However, the fast electron-hole recombination of P25 and the low efficiency of the process under visible light irradiation greatly restrict its applications in surface water, such as lakes and rivers.[15,16] In addition, most photocatalysts, such as P25, are dispersed in water; this leads to inevitable secondary pollution and low reusability. The light can hardly penetrate into deep water, so the degradation rate is very low for photocatalysts dispersed in water. In view of the drawbacks of traditional remediation techniques of oil spills, there is an urgent need to develop

Additional Supporting Information may be found in the online version of this article.

an efficient, nontoxic, recyclable, and floating photocatalyst, whose prominent superiority is *in situ* remediation under visible light irradiation without secondary treatment.

To overcome the obstacles of photocatalysts, such as TiO_2 and ZnO, numerous strategies have been adopted to improve the charge-separation efficiency and enhance the visible-light photoactivity; these include impurity doping, surface noble-metal modification, and coupling with narrow-band-gap semiconductors.[17–19] In the recent past, many researchers have focused on the coupling of graphene with TiO_2 to enhance the photocatalytic activities of TiO_2 in the visible-light region.[20–22] On the other hand, combinations of metal nanoparticles with graphene and with TiO_2 are all attractive modification techniques for enhancing photocatalytic activity under visible-light irradiation. Quite a few composites, such as Ag/P25, P25/graphene (P25/G), Ag/graphene, and even silver/P25/graphene (Ag/P25/G) nanocomposites, have been used as photocatalysts.[23–27] Through loading, P25 and silver nanoparticles are not only dispersed on the surface of graphene sheets, but some of them are wrapped by the graphene sheets. Combining Ag, P25, and graphene can enhance the photocatalytic performance because of the substantial reduction in the recombination rate of photogenerated charge carriers by the enhanced electron transport.[28] To our best knowledge, no works related to the visible-light-mediated degradation of spill oils with Ag/P25/G nanocomposites has been reported. Hence, the study of the degradation of spill oils with Ag/P25/G nanocomposite is of fundamental and practical significance.

To further increase the photocatalytic efficiency and overcome the drawbacks of photocatalysts in powder form, the choice of a suitable substrate is obviously necessary.[29,30] Recent research has focused on different kinds of supports for loading photocatalysts; these include silica, alumina, activated carbon, clay, and zeolites. In consideration of the floating properties of spill oils, floatable substrates have attracted researchers all over the globe. A floatable photocatalyst can not only maximize the illumination/light utilization process, especially in a system with solar irradiation, but it also maximizes the oxygenation of the photocatalyst by the proximity with the air/water interface, especially for nonstirred reactions.[31,32] A polyurethane (PU) sponge is a three-dimensional porous polymeric product with a low density, high porosity, high adsorption ability, and good elasticity; this makes it a good candidate for a substrate and absorbent.[33,34] Although many efforts have been made to absorb oil with PU sponges, few reports have observed the degradation of spill oils with photocatalysts based on PU sponges, let alone the adsorption and degradation of spill oils in surface water under visible-light irradiation.

Therefore, the main objectives of this study were to fabricate novel floating photocatalysts through the incorporation of Ag/P25/G nanoparticles into PU sponge and to investigate the adsorption and degradation capacity of the novel photocatalyst for diesel in surface water under visible-light irradiation. The influencing factors included the pH and temperature. The reusability of the synthesized photocatalysts was also investigated. As far as we know, this floating nanocomposite foam, with excellent reusability, is the first photocatalyst for the visible-light-mediated remediation of diesel-polluted surface water.

EXPERIMENTAL

Materials

Natural graphite flakes (325 mesh), sodium nitrate, concentrated sulfuric acid, potassium permanganate, hydrogen peroxide, concentrated hydrochloric acid, ethanol, silver nitrate, and sodium borohydride were obtained from Sigma-Aldrich Co. TiO_2 (Degussa P25), mainly composed of anatase (ca.70%) with a mean size of about 30 nm and a surface area of 40 m^2/g, was used as received. For the production of the pure PU and PU nanocomposite foams, 4,4′-diphenyl methane diisocyanate (MDI; 99.6%), polyethylene–poly(propylene glycol) (polyether polyol), 99.6%], and dichloromethane (foaming catalyst, 99.95%) were provided by Wanhua Chemical Group Co., Ltd. (China).

All working solutions were prepared by the dilution of the stock solution with deionized water. The diesel that we used was a kind of 0# diesel, and the extracting reagent was petroleum ether. The water, on which diesel floated in the degradation process, was real surface water collected from the Yangtze River in Nanjing. The water quality parameters were as follows: pH 7.6, turbidity = 118 nephelometric turbidity unit (NTU), dissolved oxygen = 5.3 mg/L, water temperature = 18–23 °C, conductivity = 300 us/cm, total nitrogen = 1.5 mg/L, total phosphorus = 0.1 mg/L, and dissolved organic carbon = 0.86 mg/L. All reagents used in the experiment were analytical grade and were used as received without further purification.

Synthesis of the Ag/P25/G Nanocomposites

Graphite oxide was obtained from natural graphite flakes (325 mesh) via a modified Hummers' method. The detailed experimental process was developed according to a previous report by Zhou *et al.*[35] The hydrothermal method described by Yang *et al.*[27] was used to synthesize the P25/G hybrid nanoparticles. Finally, silver nitrate was added to the P25/G solution; this was followed by reduction with sodium borohydride to load Ag onto the P25/G nanoparticles. Specific experimental process to obtain the Ag/P25/G nanocomposite was performed according to the study by Wen *et al.*[28]

Preparation of the Polyurethane Foams Modified with Silver/Titanium Dioxide/Graphene Ternary Nanoparticles (PU–Ag/P25/G)

One gram of the aforementioned Ag/P25/G nanocomposite was mixed with 10 g of MDI at 3900 rpm for 60 min in a flask in an oil bath at 90 °C under inert atmospheric conditions. Two grams of dichloromethane (foaming catalyst) was added to 15 g of polyethylene–poly(propylene glycol) (polyether polyol) and stirred at 3000 rpm for 25 s. The Ag/P25/G nanocomposite dispersed in MDI was cooled to room temperature and was immediately added to the polyether polyol mixture and stirred at 3000 rpm for 25 s. The resulting mixture was quickly poured into a mold and allowed to foam freely in one direction. The product was denoted as PU–Ag/P25/G-2. With the same procedure, 0.5 and 1.5 g of the Ag/P25/G nanocomposites were added to PU, and the resulting products were denoted as PU–Ag/P25/G-1 and PU–Ag/P25/G-3, respectively. The resulting foams were allowed to stand for 24 h at room temperature and

Table I. Sample Composition

Sample	Filler concentration (wt %)	Filler composition		
		P25 (wt %)	Graphene (wt %)	Ag (wt %)
PU	0	—	—	—
PU-P25	3.57	100	0	0
PU-P25/G	3.57	95.24	4.76	0
PU-Ag/P25/G-1	1.82	66.5	3.33	30.17
PU-Ag/P25/G-2	3.57	66.5	3.33	30.17
PU-Ag/P25/G-3	5.26	66.5	3.33	30.17

atmospheric pressure. In addition, PU, PU supporting P25, and PU supporting P25/G were prepared through the same procedure for comparison. The obtained samples were labeled as PU, polyurethane-foam-supported P25 (PU–P25), and polyurethane-foam-supported P25/G (PU–P25/G), respectively. The compositions of all of the samples fabricated in the experiment are listed in Table I.

Characterization

The microstructure of the foam samples was observed with scanning electron microscopy (SEM; Hitachi S-4800), and the morphology of the nanoparticles was observed with transmission electron microscopy (TEM; JEOL JEM-2010). An energy-dispersive X-ray (EDX) spectrometer fitted to an electron microscope was used for elemental analysis. Power X-ray diffraction (XRD) patterns were recorded from 10 to 90° on a Rigaku SmartLab X-ray diffractometer with Cu Kα radiation (40 kV, 100 mA). Fourier transform infrared (FTIR) spectra were recorded with an FTIR spectrometer (Bruker-Tensor 27, Germany) in the range of 4000–600 cm^{-1}. A Specord 2450 spectrometer (Shimazu Co., Japan) at wavelengths of 200–800 nm was used to test the ultraviolet–visible (UV–vis) diffuse reflectance spectra (UV–vis DRS) of the nanoparticles. The surface area of the synthesized materials was determined from N_2 adsorption–desorption isotherms with the Brunauer–Emmett–Teller (BET) method with a Micrometritics Tristar 3000 instrument. The densities of the synthesized materials were calculated according to ISO 845:2006 (E) from the measurement of the dimensions and the weight of the cubic samples.

Adsorption and Photocatalytic Degradation Experiments

We produced an expected proportion of the diesel–water mixture as a sort of simulated diesel-polluted surface water by pouring 40 g of diesel into a 500-mL beaker containing 300 mL of surface water, which was collected from the Yangtze River in Nanjing. To obtain better adsorption and degradation effects, the foams were cut into slices first. A suspension of composite foam and diesel was obtained after the addition of 0.3 g of composite foam into the beaker. The experiments were conducted at 20 ± 2 °C and an initial pH 7.0. Illumination experiments were carried out with a 500-W halogen tungsten lamp with a UV cutoff filter ($\lambda \geq 420$ nm).

The adsorption tests were conducted first. We maintained the suspension of composite foam and diesel in the dark by covering it with aluminum foil, and the beaker was placed on a shaker at 50 rpm for 15 min to reach adsorption equilibrium. Afterward, the composite foam was removed and allowed to drop the unadsorbed diesel on the foam at room temperature for 30 s. The unadsorbed excess diesel agent left in the beaker was extracted by petroleum ether. The diesel adsorption capacity was then obtained after we analyzed the concentration of the excess diesel by UV–vis spectroscopy with classical calibration methods. After that, the diesel-infiltrated foams were moved to a new diesel–water mixture solution, in which the concentration of diesel was 15 g/L. The excess diesel left in the beaker was periodically extracted by petroleum ether at 2, 4, 6, 8, 10, 12, 14, and 16 h of visible-light irradiation; then, the samples were analyzed with UV–vis spectroscopy.

To obtain the exact concentration of the excess diesel in the beaker, 0, 3, 6, 9, 12, and 15 g/L solutions of diesel were prepared with petroleum ether to obtain the standard curve. After the determination of the concentration of the excess diesel, the quality of the excess diesel was obtained, according to which the adsorption ability and degradation rate of the catalyst could be calculated easily. In detail, the diesel degradation rates at different times were calculated according to the diesel concentration at different time nodes. The reusability of the composite foam was evaluated via a repeating adsorption–pressing process followed by washing with petroleum solvent. All of the experiments were replicated three times.

RESULTS AND DISCUSSION

Morphological Characterization of the Composites

The photographic and SEM images of the pure PU and different nanocomposite foams are shown in Figure 1. Figure 1(a) shows the photographic images of the PU foam and composite foams. It was obvious that the translucent PU foam turned yellow after P25 was anchored. Similarly, the translucent PU foam turned black after the P25/G was anchored and turned gray after Ag/P25/G was anchored; this indicated an apparent distinction between these foams because of the loading of different nanoparticles. The typical SEM micrographs of PU, PU–P25, PU–P25/G, and PU–Ag/P25/G showed similar cellular structures [Figure 1(b,c)]; this implied that these nanocomposites (P25, P25/G, and Ag/P25/G) were embedded inside the polymer matrix uniformly, and their presence did not change the PU structure. The difference between the nanocomposite foams and PU was that the open pores in these foams decreased to varying degrees after different nanocomposites were anchored. Figure 1(b) shows that the surface of the pure PU seemed to be smooth with few impurities. However, in comparison, a relative

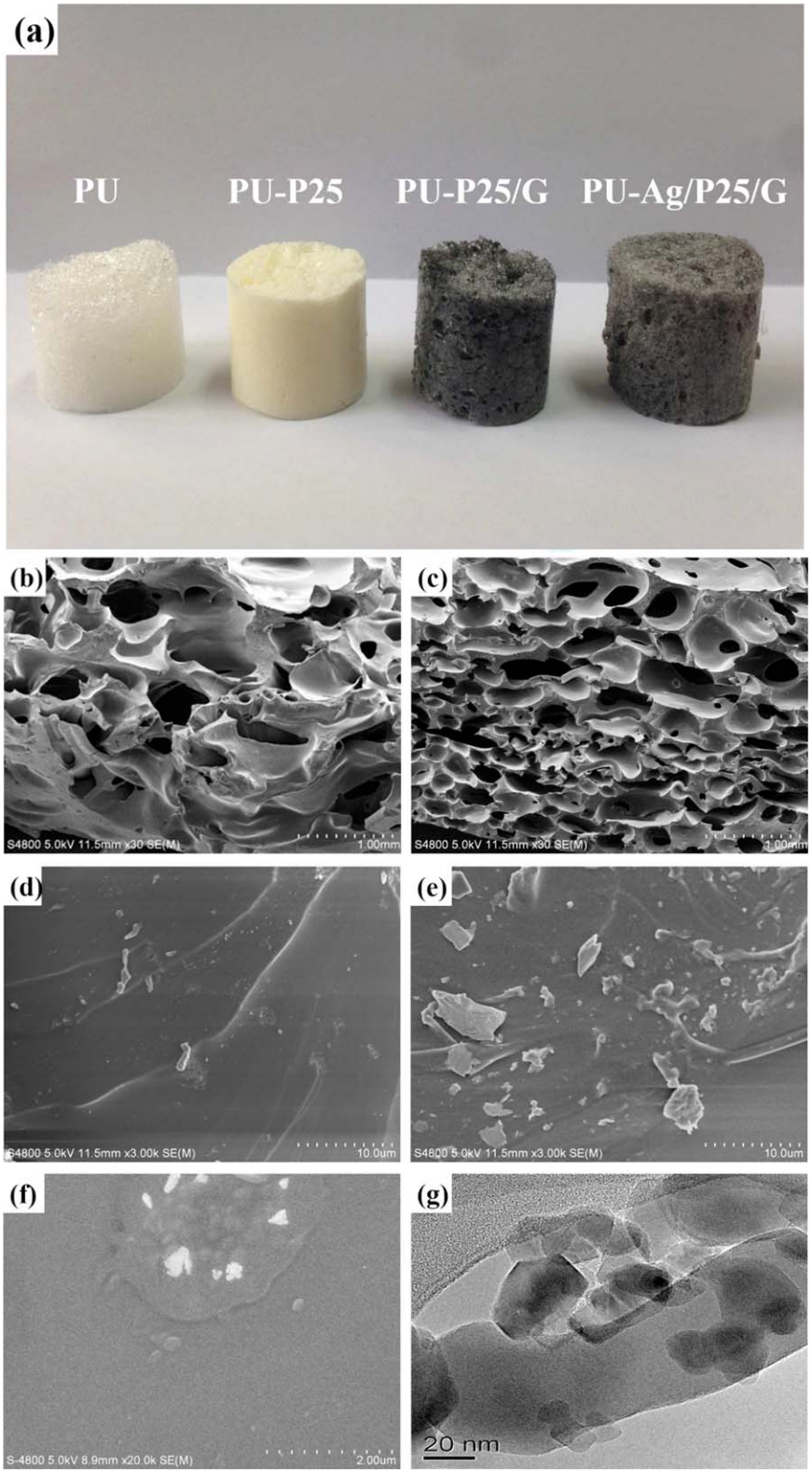

Figure 1. (a) Photographic images of the pure PU, PU–P25, PU–P25/G, and PU–Ag/P25/G-2 (from left to right), microstructural images (SEM) of the (b) pure PU, (c,d) PU–P25, (e) PU–P25/G, and (f) PU–Ag/P25/G-2 and (g) morphological image (TEM) of the Ag/P25/G-2 nanoparticles. [Color figure can be viewed in the online issue, which is available at wileyonlinelibrary.com.]

rough multilayer structure and many agglomerates of P25 crystallites of irregular size (1–2 μm) were observed in the image of PU–P25 [Figure 1(d)]. It is shown in Figure 1(e) that graphene had a crumpled layered structure composed of several stacking layers of graphene sheets, and some of the graphene sheets were broken into small pieces during the preparation process. Furthermore,

Table II. EDX Analysis of the Pure PU, PU–P25, PU–P25/G, and PU–Ag/P25/G-2

	Ti		Ag	
	wt %	atom %	wt %	atom %
PU	0	0	0	0
PU-P25	14.87	4.46	0	0
PU-P25/G	11.54	3.37	0	0
PU-Ag/P25/G-2	4.21	14.1	0.35	0.05

the SEM micrographs of PU–Ag/P25/G [Figure 1(f)] showed that the graphene sheets were decorated by nanoparticles in matrix and on the surface of the polymer. To investigate the morphology of the nanoparticles, TEM micrograph of the Ag/P25/G-2 nanoparticles is shown in Figure 1(g). Some nanoparticles were dispersed unevenly on the graphene nanosheets, and a little aggregation spread on the graphene scaffold. To further analyze the component of the nanoparticles, EDX spectrometry was conducted.

The results of EDX shown in Table II reveal that both Ag and P25 could be detected in PU–Ag/P25/G-2 with random selection. The weight percentages of Ag and Ti were tested to be 0.35 and 4.21%, respectively. The weak elemental Ag and P25 peaks in this spectrum also indicated the successful synthesis of PU–Ag/P25/G. Nevertheless, only titanium could be seen in PU–P25 and PU–P25/G, with titanium weight percentages of 14.87 and 11.54%, respectively. As predicted, there was no silver or titanium detected in the pure PU according to Table II. Detailed EDX spectra of samples are shown in Figure S1 (Supporting Information).

Figure 2 shows the XRD patterns of the PU–Ag/P25/G [Figure 2(a)], PU–P25/G [Figure 2(b)], PU–P25 [Figure 2(c)], and pure PU [Figure 2(d)] samples. The diffractogram showed peaks at 2θ values of 25.3, 37.8, 48.0, 53.9, 55.1, 62.7, 68.8, 70.3, and 75.0°; these were assigned to the anatase (101), (004), (200), (105), (211), (204), (116), (220), and (215) crystal planes. In addition, characteristic diffraction peaks at 27.4, 36.1, and 41.2° also appeared; these were attributed to the (110), (101), and (111) faces of the rutile TiO_2, respectively. No diffraction patterns of graphene were detected. One possible reason was that the particular peak of graphene at 25° was shielded by the main anatase (101) peak at 25.3°. The diffraction peaks for Ag at 2θ values of 44.4 and 64.4° were assigned to the (200) and (220) planes of the cubic structure of Ag; this improved the successful reduction of silver nitrate under solvothermal conditions. A separate peak for Ag at a 2θ value of 38.1° was inconspicuous; this was probably due to the presence of the anatase (004) peak at 37.8°. Another peak at 77.4° ascribed to the Ag (311) plane was not displayed because of the low amount of added silver nitrate. It could also be inferred that the average crystallite size of the P25 nanoparticles remained unaltered after the loading of silver nanoparticles. Moreover, a broad curve between 15 and 25° attributed to PU accounted for the amorphization and lower degree of crystallinity of PU.

The optical response of the Ag/P25/G nanoparticles was tested by UV–vis spectroscopic measurement. As shown in Figure 3, the

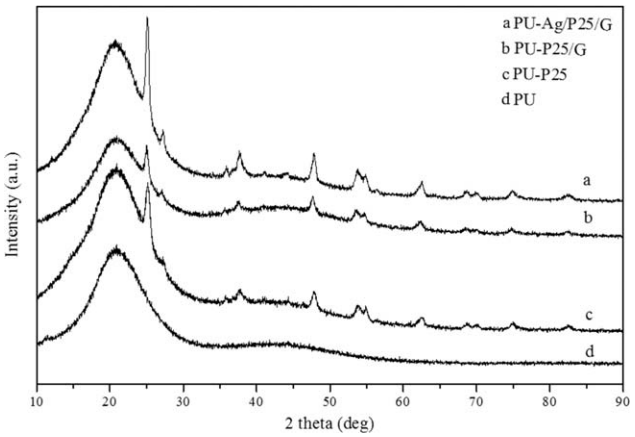

Figure 2. XRD patterns of the (a) PU–Ag/P25/G, (b) PU–P25/G, (c) PU–P25, and (d) pure PU.

optical adsorption of the pure P25 was weak in the visible-light region, and there was an adsorption edge around 330 nm, which was ascribed to the band-to-band transition of anatase TiO_2. The enhanced adsorption of P25/G in the region greater than 350 nm was attributed to the presence of graphene; this was also observed in the curve of the Ag/P25/G nanocomposite. After combination with graphene, the adsorption edge of P25/G had a significant red-shift to 456 nm. It could be explained that the chemical bonding between P25 and graphene narrowed the band gap of P25 because of the formation of the Ti—O—C band.[36] Furthermore, in the curve of Ag/P25/G, a broad adsorption band from 400 to 550 nm appeared. Such a band further proved the successful introduction of silver nanoparticles on account of the reduction of Ag^+ ions by sodium borohydride.[15] The photocatalytic activity of PU–Ag/P25/G was expected to improve with the broad adsorption of the Ag/P25/G nanocomposites extending into visible-light region. From the results of SEM, EDX, XRD, and UV–vis spectroscopic measurements, we concluded that the ternary Ag/P25/G hybrid was successfully prepared, and the three components were assembled homogeneously on PU foams. Notably, ternary PU-based nanocomposites foams with such uniform structural features are scarce in the literature. The FTIR spectroscopy study of the prepared

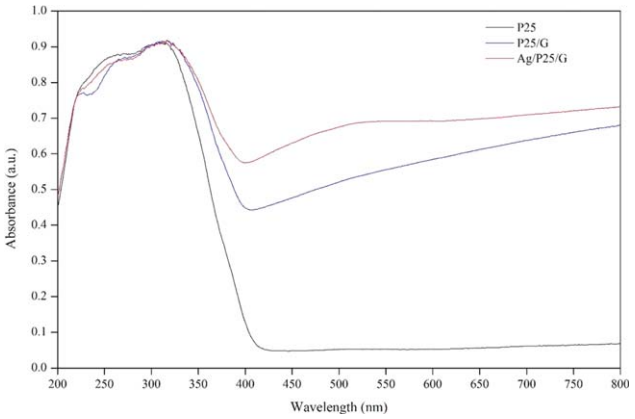

Figure 3. UV–vis diffuse reflection spectra of P25, P25/G, and Ag/P25/G. [Color figure can be viewed in the online issue, which is available at wileyonlinelibrary.com.]

Table III. Densities and BET Surface Areas of the Pure PU and PU-Based Nanocomposite Foams

Sample	Density (g/cm^3)	BET surface area (m^2/g)
PU	0.12	7
PU-P25	0.17	11
PU-P25/G	0.20	14
PU-Ag/P25/G-1	0.22	10
PU-Ag/P25/G-2	0.26	14
PU-Ag/P25/G-3	0.31	12

photocatalyst confirmed the main structure of the obtained nanocomposite foams (Figure S2, Supporting Information). The spectroscopic features of PU–Ag/P25/G, PU–P25/G, and PU–P25 were similar to that of the pure PU after different nanoparticle depositions, as indicated in Figure S2; this suggested that the loading of the nanoparticles did not change the structure of the PU foam.

Table III shows that the density of all of the samples were much lower than that of water (1.0 g/cm^3) because of the creation of abundant empty holes during the preparation process; this ensured the floating properties of the photocatalysts. The density increased continuously and in an orderly fashion with the modification of P25, P25/G, and Ag/P25/G, and the increasing amount of the Ag/P25/G nanocomposite apparently resulted in increases in the sample densities. Table III also indicated that the surface area increased strongly after the incorporation of P25 into PU foams; this could have been related to the formation of a highly dispersed porous P25 phase. Additionally, the surface area increased to a higher degree with the modification of P25/G; this was caused by the reduction of the agglomeration of P25 nanoparticles. The surface area of PU–Ag/P25/G decreased with the incorporation of a higher content of Ag/P25/G nanoparticles; this could be explained that the pores inside the composite foam decreased when Ag/P25/G nanoparticles were overdosed.

Adsorption Capacity of the Prepared Nanocomposite Foams for Diesel

As shown in Table III, this indicated that the prepared nanocomposite foams had a low density and high porosities so that the ability of diesel adsorption was a critical factor for the photocatalysts in the photocatalytic process. The adsorption capacity of the samples was measured under dynamic conditions to simulate real surface water conditions. As shown in Figure 4, the adsorption capacity increased markedly after the modification of different nanocomposites on PU. The stronger affinity for oil of PU–P25 was regarded as evidence for the contribution of P25 nanoparticles to the hydrophobicity and oleophilicity of the modified PU. Analogously, the adsorption capacity of the PU–P25/G foam was further increased with the addition of the enhanced adsorption properties of P25/G nanoparticles; this was attributed to the fact that graphene effectively prevented the P25 nanoparticles from agglomerating. No obvious enhancement of the adsorption capacity was obtained with further modification with Ag, according to the curve of

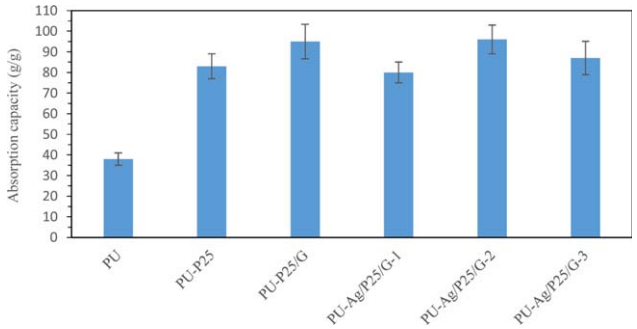

Figure 4. Adsorption capacity of the prepared nanocomposite foams for diesel. [Color figure can be viewed in the online issue, which is available at wileyonlinelibrary.com.]

PU–Ag/P25/G-2. It is worth noting that the adsorption capacity of PU–Ag/P25/G significantly decreased with increasing amount of Ag/P25/G nanoparticles to 1.5 g; this could be explained by the fact that too much Ag/P25/G nanoparticles surely clogged the macroporous foams and decreased the open cells of PU–Ag/P25/G by a large margin. According to Table III, the adsorption capacity of the nanocomposite foams was almost consistent with the results of the BET surface area measurements.

Photodegradation of the Prepared Nanocomposite Foams for Diesel under Visible Light

The photocatalytic activity of the prepared catalyst was investigated with visible-light irradiation after we obtained the dark adsorption equilibrium. Except for the use of real surface water, the reactions were carried out under dynamic conditions at an equilibrium temperature of 20 ± 2 °C and a pH of 7.0. The kinetic profiles of diesel photocatalysis in the water phase are shown in Figure 5.

As shown in Figure 5, the degradation rate of diesel increased rapidly from 0 to 14 h of the whole reaction time, and the degradation process slowed down gradually in the following 2 h. The

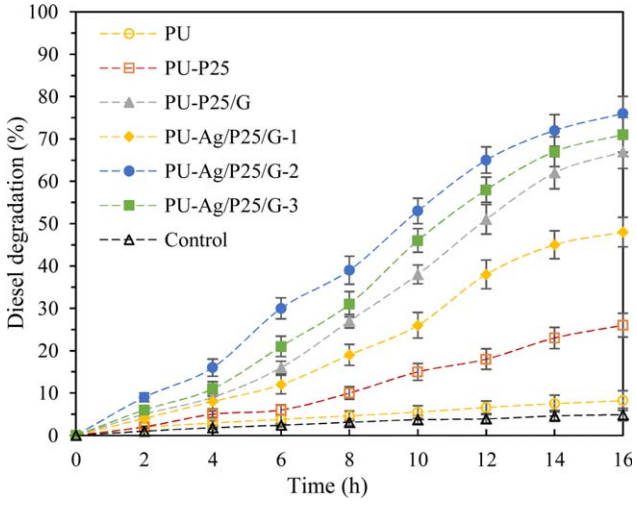

Figure 5. Photodegradation of the prepared nanocomposite foams for diesel under visible-light irradiation. [Color figure can be viewed in the online issue, which is available at wileyonlinelibrary.com.]

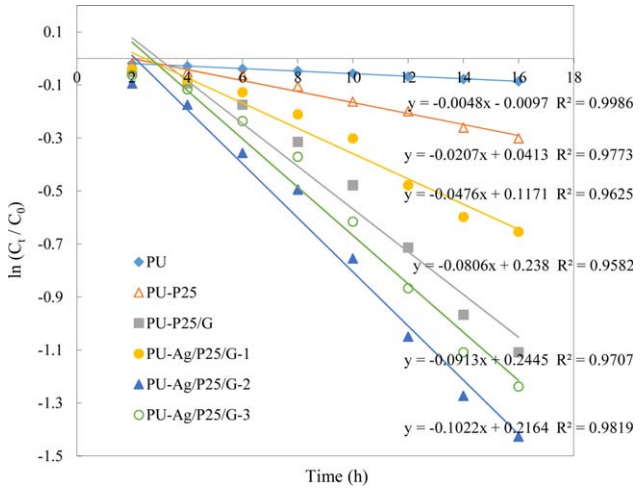

Figure 6. First-order kinetic model of diesel degradation by visible-light irradiation with various photocatalysts. [Color figure can be viewed in the online issue, which is available at wileyonlinelibrary.com.]

degradation rate order of the prepared catalysts was PU–Ag/P25/G > PU–P25/G > PU–P25 > Pure PU. There was a small loss of diesel because of the volatilization during the reaction without the use of the photocatalyst.

Because of the poor activation in the visible-light region, the diesel degradation rate of PU–P25 was only 26%. In contrast, the degradation rate of PU–P25/G was 67%; this was much higher than that of PU–P25. This was attributed to the presence of graphene, which improved the light adsorption intensity, extended the light adsorption range, and enhanced the transportation of the photogenerated charge carriers. Specifically, P25 could be illuminated by visible light in the presence of graphene. Electrons were promoted from the valence band to the conduction band to give electron-hole pairs. Hydroxyl radical generated from the valence band was an oxidizing agent and was powerful enough to oxidize the organic compound in diesel. The excited electron could react with an organic molecule directly, and this reduced the pollutant. In addition, the excited electron reacted with oxygen to produce a superoxide anion radical, which reacted with the pollutant or formed a hydroperoxyl radical. Through some steps, hydroperoxyl radicals can eventually yield hydroxyl radicals.

PU–Ag/P25/G exhibited much higher photocatalytic activities than PU–P25/G and PU–P25 when the same amount of nanoparticles were added, as shown in Figure 5. In visible-light irradiation, silver nanoparticles remarkably suppressed the recombination of photoelectron-hole pairs; thus, more hydroxyl radicals and excited electrons were generated to degrade organic compounds in diesel. On this account, the diesel degradation was facilitated, and the photocatalytic performance of PU–Ag/P25/G was enhanced.

On the basis of the curves of PU–Ag/P25/G-1 and PU–Ag/P25/G-2 in Figure 5, the degradation rate increased with increasing modification rate of Ag/P25/G on PU. This seemed to be due to the increase in the BET surface area and the higher amount of active photocatalytic sites; it resulted in a 28% higher degradation in the case of PU–Ag/P25/G-2 compared with PU–Ag/P25/G-1. On the other hand, according to the curve of PU–Ag/P25/G-3, the degradation rate significantly decreased to 71%; this was probably due to the overdose of Ag/P25/G nanoparticles. The amount of active photocatalytic sites could be decreased when Ag/P25/G was overdosed because of the decreased visible-light penetration, increased light scattering, and losses in open cells and the adsorption capacity of PU–Ag/P25/G caused by the agglomeration of Ag/P25/G nanoparticles at a high modified concentration.

The experimental data was fitted to the apparent first-order kinetic model (1), where k_{ap} is the apparent rate constant (min^{-1}), C_t is the reaction concentration of diesel and C_0 is the initial concentration at time $(t) = 0$:

$$-\ln(C_t/C_0) = k_{ap}t \quad (1)$$

The results were also plotted as the natural log of the concentration ratio $\ln(C_t/C_0)$ versus the time (Figure 6).The results indicate that the degradation was directly related to the various photocatalysts used in the reactions because the data exhibited the best fit in the case of the first-order kinetic model because of the high correlation coefficient values. The slope value followed the order PU–Ag/P25/G-2 > PU–Ag/P25/G-3 > PU–P25/G > PU–Ag/P25/G-1 > PU–P25 > PU; this was consistent with the diesel degradation rate order for the various photocatalysts.

Effect of pH on the Photocatalytic Degradation of Diesel

In a heterogeneous photoreaction, the pH of the solution is an important variable in aqueous-phase-mediated photocatalytic reactions. In this test, the solution initial pH was controlled in the range 5.5–8.5. Figure 7 shows that curves of the three photocatalysts were similar, and the degradation rate of PU–Ag/P25/G increased constantly with increasing pH value of the solution; this was due to the change in the binding between the nanocomposite foams and diesel.[37] A large drop in degradation by PU–Ag/P25/G was observed when the initial pH was set in the alkaline range (8.0–8.5); this could be regarded as the result

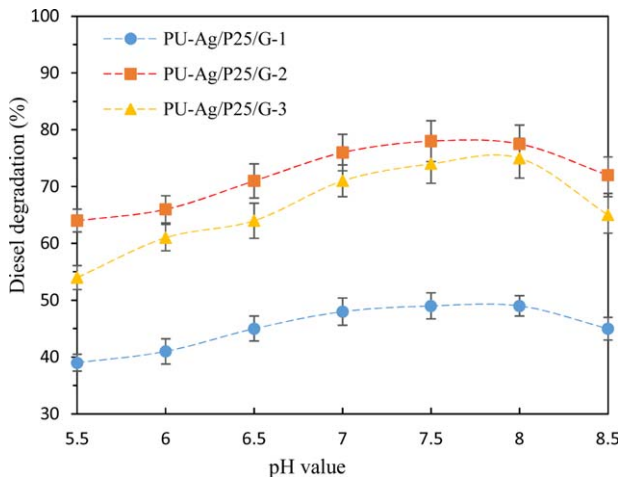

Figure 7. Effect of the pH on the degradation rate of diesel removal by PU–Ag/P25/G under visible-light irradiation for 16 h. [Color figure can be viewed in the online issue, which is available at wileyonlinelibrary.com.]

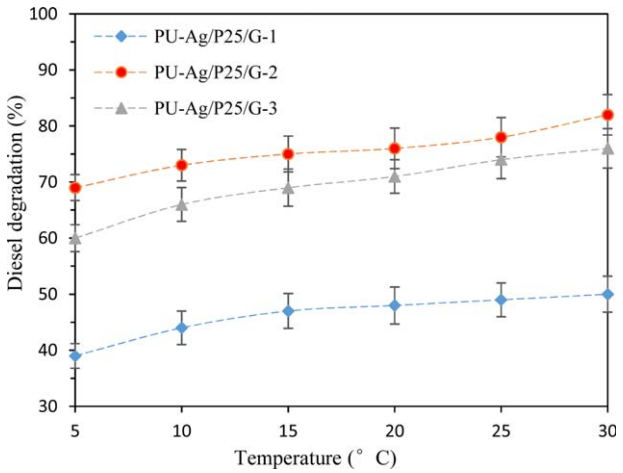

Figure 8. Effect of the temperature on the degradation rate of diesel removal by PU–Ag/P25/G under visible-light irradiation for 16 h. [Color figure can be viewed in the online issue, which is available at wileyonlinelibrary.com.]

of the desorption effect, that diesel did not adsorb onto the negatively charged surface of the photocatalysts. The highest efficiency of degradation by PU–Ag/P25/G was at pH 7.5–8.0; this was consistent with the pH of the surface water. In the pH range 7.5–8.0, the electrostatic attraction between the positively charged Ag/P25/G and negatively charged diesel led to strong interaction in PU–Ag/P25/G. It could also be deduced from Figure 7 that the addition of a larger amount of Ag/P25/G nanoparticles showed a clear effect from the pH of the Ag/P25/G nanoparticles. All of the results illustrate the fact that the active property of the photocatalyst was also affected by the adjustment of the solution pH value. Because PU is chemically resistant to acid and alkali, PU–Ag/P25/G could be used as an industrial photocatalyst for the effective treatment of spilled oil.

Effect of the Temperature on the Photocatalytic Degradation of Diesel

To determine the effect of the temperature on the degradation of diesel, several experiments were conducted at different temperatures ranging from 5 to 30 °C (approximating the average temperature of surface water in summer; Figure 8). As shown in Figure 8, with increasing temperature of the suspension solution from 5 to 30 °C, the degradation rate increased smoothly. According to the slight effect of the temperature, the viscosity of diesel, which decided the pore filling, decreased with the reduction in the temperature of the suspension solution. Obviously, the adsorption effect of diesel on the PU–Ag/P25/G weakened because the degradation rate of diesel was affected indirectly. We speculated that the greater degradation rate of diesel could be obtained when the photocatalytic process was conducted in warm surface water in summer than in cold water in winter.

Reusability Test of the PU–Ag/P25/G Photocatalyst

The regeneration and reusability of a photocatalyst in the degradation process can be regarded as one of the most important factors in the selection of a photocatalyst for practical application.[38] In this study, the stability and reusability of the photocatalysts were investigated with PU–Ag/P25/G-1, PU–Ag/P25/G-2, and PU–Ag/P25/G-3 submitted to five consecutive reactions under visible-light irradiation. After each reaction, the photocatalyst was recovered with a simple squeezing process; this was followed by washing with petroleum solvent, and a new diesel floating solution was used.

After five reactions, the photocatalysts were still active with the degradation rate of PU–Ag/P25/G-1, PU–Ag/P25/G-2, and PU–Ag/P25/G-3 measured at 42, 71, and 64%, respectively. The photocatalysts exhibited an almost similar degradation ability in the other four cycles under the same conditions with minor changes in efficiency. The slight decrease in the degradation of diesel was probably due to the adhesion of diesel in the pores and surface of the foams. These results clearly indicate that the floating photocatalyst PU–Ag/P25/G could be reused at least several times without a significant loss in photocatalytic activity. To summarize, the nanoparticles of Ag/P25/G showed little tendency to be cleaved from the surface of the PU foam during the photocatalytic process, and the graft between the PU and Ag/P25/G nanoparticles was very compact and solid; this facilitated reusability.

CONCLUSIONS

In this study, a novel floating photocatalyst, PU–Ag/P25/G, was synthesized by the loading of Ag/P25/G nanoparticles onto the PU foams. The characterization results revealed the nanoscale dispersion of the Ag/P25/G nanoparticles in matrix and on the surface of the PU foam. The visible-light degradation experiments indicated that the absorbability (96 g/g) and diesel degradation capacity (76%) of PU–Ag/P25/G in surface water were the highest among the as-synthesized pure PU and PU–P25, PU–P25/G, and PU–Ag/P25/G. The efficiency of diesel degradation by PU–Ag/P25/G was enhanced with increasing temperature of the solution from 5 to 30 °C, and the optimum pH was from 7.5 to 8.0. Furthermore, the novel photocatalyst could be used at least five times with a continuous high diesel degradation efficiency; this showed its potential application value in surface water restoration.

REFERENCES

1. Al-Majed, A. A.; Adebayo, A. R.; Hossain, M. E. *J. Environ. Manage.* **2012**, *113*, 213.
2. Wang, D.; Silbaugh, T.; Pfeffer, R.; Lin, Y. S. *Powder Technol.* **2010**, *203*, 298.
3. Shi, X. Y.; He, K. B.; Song, W. W.; Wang, X. T.; Tan, J. H. *Front. Env. Sci. Eng.* **2012**, *6*, 463.
4. Zhang, X. Y.; Wang, Z. Z.; Liu, X. Y.; Hu, X.; Liang, X.; Hu, Y. *Int. Biodeter. Biodegrad.* **2013**, *76*, 71.
5. Chandran, P.; Das, N. *Biodegradation* **2011**, *22*, 1181.
6. Dave, D.; Ghaly, A. E. *Am. J. Environ. Sci.* **2011**, *7*, 423.
7. D'Auria, M.; Emanuele, L.; Racioppi, R.; Velluzzi, V. *J. Hazard. Mater.* **2009**, *164*, 32.
8. Garcia-Martinez, M. J.; Da Riva, I.; Canoira, L.; Llamas, J. F.; Alcantara, R.; Gallego, J. L. R. *Appl. Catal. B* **2006**, *67*, 279.
9. Santos, F. V.; Azevedo, E. B.; Sant'Anna, G. L.; Dezotti, M. *Braz. J. Chem. Eng.* **2006**, *23*, 451.

10. King, S. M.; Leaf, P. A.; Olson, A. C.; Ray, P. Z; Tarr, M. A. *Chemosphere* **2014**, *95*, 415.
11. Wong, M. S.; Jeng, E. S.; Ying, J. Y. *Nano Lett.* **2001**, *1*, 637.
12. Fan, J. J.; Zhao, L.; Yu, J. G.; Liu, G. *Nanoscale* **2012**, *4*, 6597.
13. Emam, E. A.; Aboul-Gheit, N. A. K. *Energy Sources A* **2014**, *36*, 1123.
14. Vargas, R.; Nunez, O. *Sol. Energy* **2010**, *2*, 345.
15. Herrmann, J. M. *Catal. Today* **1999**, *53*, 115.
16. Chen, X. B.; Mao, S. S. *Chem. Rev.* **2007**, *107*, 2891.
17. Graciani, J.; Alvarez, L. J.; Rodriguez, J. A.; Sanz, J. F. *J. Phys. Chem. C* **2008**, *112*, 2624.
18. Subramanian, V.; Wolf, E. E.; Kamat, P. V. *J. Am. Chem. Soc.* **2004**, *126*, 4943.
19. Chen, X. B.; Liu, L.; Yu, P. Y.; Mao, S. S. *Science* **2011**, *331*, 746.
20. Zhang, J. T.; Xiong, Z. G.; Zhao, X. S. *J. Mater. Chem.* **2011**, *21*, 3634.
21. Sun, L.; Zhao, Z. L.; Zhou, Y. C.; Liu, L. *Nanoscale* **2012**, *4*, 613.
22. Akhavan, O.; Ghaderi, E. *J. Phys. Chem.* **2009**, *113*, 20214.
23. Li, Y. Z.; Zhang, H.; Guo, Z. M.; Han, J. J.; Zhao, X. J.; Zhao, Q. N.; Kim, S. J. *Langmuir* **2008**, *24*, 8351.
24. Awazu, K.; Fujimaki, M.; Rockstuhl, C.; Tominaga, J.; Murakami, H.; Ohki, Y.; Yoshida, N.; Watanabe, T. *J. Am. Chem. Soc.* **2008**, *130*, 1676.
25. Pasricha, R.; Gupta, S.; Srivastava, A. K. *Small* **2009**, *5*, 2253.
26. Wu, T. S.; Liu, S.; Luo, Y. L.; Lu, W. B.; Wang, L.; Sun, X. P. *Nanoscale* **2011**, *3*, 2142.
27. Yang, Y. H.; Liu, E. Z.; Dai, H. Z.; Kang, L. M.; Wu, H. T.; Fan, J.; Hu, X. Y.; Liu, H. C. *Int. J. Hydrogen Energy* **2014**, *39*, 7664.
28. Wen, Y. Y.; Ding, H. M.; Shan, Y. K. *Nanoscale* **2011**, *3*, 4411.
29. Singh, S.; Mahalingam, H.; Singh, P. K. *Appl. Catal. A* **2013**, *462*, 178.
30. Lee, L. J.; Zeng, C. C.; Cao, X.; Han, X. M.; Shen, J. *Compos. Sci. Technol.* **2005**, *65*, 2344.
31. Xing, Z. P.; Li, J. Z.; Wang, Q.; Zhou, W.; Tian, G. H.; Pan, K.; Tian, C. G.; Zou, J. L.; Fu, H. G. *Eur. J. Inorg. Chem.* **2013**, *13*, 2411.
32. Chen, S. F.; Cao, G. Y. *Sol. Energy* **2005**, *79*, 1.
33. Duong, H. T. T.; Burford, R. P. *J. Appl. Polym. Sci.* **2009**, *99*, 360.
34. Li, H.; Liu, L. F.; Yang, F. L. *Mar. Pollut. Bull.* **2012**, *64*, 1648.
35. Zhou, Q.; Zhong, Y. H.; Chen, X.; Liu, J. H.; Huang, X. J.; Wu, Y. C. *J. Mater. Sci.* **2014**, *49*, 1066.
36. Ren, W. J.; Ai, Z. H.; Jia, F. L.; Zhang, L. Z.; Fan, X. X.; Zou, Z. G. *Appl. Catal. B* **2007**, *69*, 138.
37. Mahalakshmi, M.; Priya, S. V.; Arabindoo, B.; Palanicharnly, M.; Murugesan, V. *J. Hazard. Mater.* **2009**, *161*, 336.
38. Nikkhah, A. A.; Zilouei, H.; Asadinezhad, A.; Keshavarz, A. *Chem. Eng. J.* **2015**, *262*, 278.